CHAPTER 6

Light-induced termination of spiral wave arrhythmias by optogenetic engineering of atrial cardiomyocytes

Brian O. Bingen, MD[1,†]; Marc C. Engels, MD[1,†]; Martin J. Schalij, MD, PhD[1]; Wanchana Jangsangthong, PhD[1]; Zeinab Neshati, MSc[1]; Iolanda Feola, MSc[1]; Dirk L. Ypey, PhD[1]; Saïd F.A. Askar, PhD[1]; Alexander V. Panfilov, PhD[2]; Daniël A. Pijnappels, PhD[1,†]; Antoine A.F. de Vries, PhD[1,†]

[†]These authors contributed equally to this work.

[1]Laboratory of Experimental Cardiology, Department of Cardiology, Heart Lung Center Leiden, Leiden University Medical Center, Leiden, the Netherlands.
[2]Department of Physics and Astronomy, Ghent University, Ghent, Belgium.

Adapted from: Cardiovascular Research. 2014;104:194-205.

Abstract

Aims Atrial fibrillation (AF) is the most common cardiac arrhythmia and often involves reentrant electrical activation (e.g. spiral waves). Drug therapy for AF can have serious side effects including proarrhythmia, while electrical shock therapy is associated with discomfort and tissue damage. Hypothetically, forced expression and subsequent activation of light-gated cation channels in cardiomyocytes might deliver a depolarizing force sufficient for defibrillation, thereby circumventing the aforementioned drawbacks. We therefore investigated the feasibility of light-induced spiral wave termination through cardiac optogenetics.

Methods and results Neonatal rat atrial cardiomyocyte monolayers were transduced with lentiviral vectors encoding light-activated Ca^{2+}-translocating channelrhodopsin (CatCh; LV.CatCh∼eYFP↑) or eYFP (LV.eYFP↑) as control, and burst-paced to induce spiral waves rotating around functional cores. Effects of CatCh activation on reentry were investigated by optical and multi-electrode array (MEA) mapping. Western blot analyses and immunocytology confirmed transgene expression. Brief blue light pulses (10 ms/470 nm) triggered action potentials only in LV.CatCh∼eYFP↑-transduced cultures, confirming functional CatCh-mediated current. Prolonged light pulses (500 ms) resulted in reentry termination in 100% of LV.CatCh∼eYFP↑-transduced cultures (n = 31) vs. 0% of LV.eYFP↑-transduced cultures (n = 11). Here, CatCh activation caused uniform depolarization, thereby decreasing overall excitability (MEA peak-to-peak amplitude decreased 251.3 ± 217.1 vs. 9.2 ± 9.5 μV in controls). Consequently, functional coresize increased and phase singularities (PSs) drifted, leading to reentry termination by PS–PS or PS–boundary collisions.

Conclusion This study shows that spiral waves in atrial cardiomyocyte monolayers can be terminated effectively by a light-induced depolarizing current, produced by the arrhythmogenic substrate itself, upon optogenetic engineering. These results provide proof-of-concept for shockless defibrillation.

Introduction

Atrial fibrillation (AF) is the most common cardiac rhythm disorder in clinical practice, substantially contributing to morbidity and mortality, especially in the elderly.[1] Yet, knowledge about its underlying mechanisms remains far from complete, although reentrant conduction is widely accepted to play a prominent role in AF. Still, current treatment of AF is suboptimal.[1–3] To convert AF to normal cardiac rhythm, drug treatment and/or electrical cardioversion are being employed. Drug treatment is rather ineffective and may have dangerous side effects such as the occurrence of ventricular arrhythmias, while electrical cardioversion is associated with tissue damage and serious discomfort. This makes the use of external or implantable cardioverter/defibrillator devices in AF treatment undesirable, as most patients would require multiple shocks per day causing electrical cardioversion to serve as a last resort treatment modality only.[4] Hence, a search for an effective, but less painful and shockless method of cardioversion is warranted.

Electrical cardioversion relies on synchronous depolarization of large areas of the atrial myocardium, in order to terminate the reentrant conduction underlying fibrillation.[5] In theory, shockfree cardioversion might be elicited by genetically modifying the atrial cardiomyocytes to express depolarizing cation channels that are activated through other means than electroshock, granted that the endogenous electrochemical gradients provide sufficient depolarizing force. Recently, optogenetics has been introduced as a method combining genetic engineering with light stimulation to control, with very high spatial and temporal resolution, specific cellular properties,[6] including the membrane potential of excitable cells.[7–9] To this end, light-gated ion channels from the microbial opsin family are expressed in target cells like cardiomyocytes or neurons, and subsequently activated by light of defined wavelengths to generate a controllable ion current. This strategy has previously been proved to be effective for light-induced pacing of ventricular cardiomyocytes following the forced expression of depolarizing light-gated channels in these cells.[8] Hence, optogenetics might provide a feasible combination of cation channels and mode of activation to achieve shock-free cardioversion. Still, it is unknown whether optogenetic engineering of atrial cardiomyocytes (aCMCs) allows for light-induced termination of fibrillation maintained by reentrant spiral waves.

Therefore, we investigated whether by optogenetic modification of aCMCs, a depolarizing photocurrent (i.e. an ion current elicited by light) could be generated sufficiently strong to terminate reentrant conduction in monolayer cultures of these cells. To this purpose, we employed Ca^{2+}-translocating channelrhodopsin (CatCh),[10] an ultra-sensitive light-gated cation channel, and a blue (470 nm) light-emitting diode (LED)-based light source for its activation. The effects of CatCh activation on reentrant conduction were investigated by voltage-sensitive dye and multi-electrode array (MEA) mapping in a 2D monolayer model of spiral wave reentry using neonatal rat aCMCs.[11]

Methods

Animal studies

All animal experiments were approved by the Animal Experiments Committee of the Leiden University Medical Center and conformed to the Guide for the Care and Use of Laboratory Animals as stated by the US National Institutes of Health.

Cell isolation and culture

Neonatal rat aCMCs were isolated as described previously.[11] Briefly, 2-day-old Wistar rats were anaesthetized by 5% isoflurane inhalation and adequate anaesthesia was confirmed by the absence of reflexes. Hearts were rapidly excised and atria were carefully separated from the ventricles. Next, atrial tissue was minced and dissociated with collagenase type 1 (450 U/mL; Worthington, Lakewood, NJ, USA) and DNase I (18.75 Kunitz/mL; Sigma-Aldrich, St Louis, MO, USA) and pre-plated on Primaria-coated cell-culture dishes (Becton Dickinson, Breda, the Netherlands) for 120 min to allow selective attachment of non-myocytes (mainly cardiac fibroblasts). Unattached cells (mainly aCMCs) were seeded in 24-well cell-culture plates (Corning Life Sciences, Amsterdam, the Netherlands) containing fibronectin (Sigma-Aldrich)-coated, round glass coverslips (15 mm diameter). Cell densities of 0.5–8 $\times$ 10^5 cells/well were used depending on the assay. At Day 1 of culture, cells were incubated with Mitomycin-C (10 µg/mL; Sigma-Aldrich) for 2 h, as described previously.[12] The culture medium, which consisted of Dulbecco's modified Eagle's medium/HAM's F10 (1: 1, v/v; Life Technologies, Bleiswijk, the Netherlands) supplemented with 5% horse serum (Life Technologies), was refreshed daily and cells were cultured in a humidified incubator at 37°C and 5% CO_2.

Construction of self-inactivating lentiviral vector shuttle plasmids

The CatCh-encoding self-inactivating lentiviral vector (SIN-LV) shuttle plasmid pLV-CaMKIIa-hChR2(L132C)-eYFP.WPRE was kindly provided by the Stanford Optogenetics Resource Center (http://www.stanford.edu/group/dlab/optogenetics). To allow generation of SIN-LVs directing high-level *CatCh* expression in aCMCs, the murine *calcium/calmodulin-dependent protein kinase II alpha* promotor in pLV-CaMKIIa-hChR2(L132C)-eYFP.WPRE was replaced by a polymerase chain reaction (PCR) fragment encoding the striated muscle-specific MHCK7 promotor.[13] The MHCK7 promoter was amplified with VELOCITY DNA polymerase (GC Biotech, Alphen aan den Rijn, the Netherlands) from a derivative of plasmid LV.ΔPRE.pA+.MHCK7.Luc[14] using deoxyribonucleotides A117 (5′ CCTTAATTAACCCTTCAGATTAAAAATAACTGA 3′) and A118 (5′ TTACCGGTGCTGGCTGGCTCCTGA 3′; Sigma-Aldrich) as forward and reverse primer, respectively. Subcloning was done using the restriction enzymes PacI and AgeI-HF (both from New England Biolabs, Ipswich, MA, USA), recognition sequences of which were

introduced at both ends of the MHCK7 promoter fragment by the PCR procedure. This yielded the SIN-LV shuttle plasmid pLV.MHCK7.CatCh~eYFP.WHVPRE. For making a negative control vector, pLV.MHCK7.CatCh~eYFP.WHVPRE was incubated with AgeI-HF and BoxI (Thermo Fisher Scientific, Waltman, MA, USA), treated with Klenow polymerase (Thermo Fisher Scientific) and the resulting 10.0 kb DNA fragment was self-ligated yielding pLV.MHCK7.eYFP.WHVPRE. The correctness of the SIN-LV shuttle constructs was verified by restriction mapping with five different enzymes and by partial nucleotide sequence analysis using the Quick Shot sequencing services of BaseClear (Leiden, the Netherlands). For large-scale purification of the SIN-LV shuttle and packaging plasmids, the JETSTAR 2.0 Plasmid Maxiprep kit (Genomed, Löhne, Germany) was used following the instructions of the manufacturer.

SIN-LV production

LV.CatCh~eYFP↑ and LV.eYFP↑ particles were produced from the SIN-LV shuttle plasmids pLV.MHCK7.CatCh~eYFP.WHVPRE and pLV.MHCK7.eYFP.WHVPRE, respectively, using a previously described method.[11] The concentrated vector suspensions were aliquoted in 100 µL portions and stored at −80°C until use. aCMCs were transduced at Day 4 of culture by adding vector suspension directly to the culture medium. After 18 h, cells were washed once with phosphate-buffered saline (PBS) and given fresh culture medium. The SIN-LVs were applied at doses that resulted in the transduction of essentially all aCMCs. Transduction level was assessed by enhanced yellow fluorescent protein (eYFP) visualization with an Axiovert 200 M inverse fluorescence microscope (Carl Zeiss, Sliedrecht, the Netherlands).

Immunocytology

Cultures were stained with antibodies directed against α-actinin (mouse IgG1, clone EA-53; Sigma-Aldrich), collagen type 1 (rabbit IgG; Abcam, Cambridge, MA, USA, ab292), connexin 43 (Cx43; rabbit Ig; Sigma-Aldrich, C6219), and atrial myosin light chain 2 (MLC2a; a gift from Dr. S.W. Kubalak, Charleston, SC, USA)[15] after fixation in PBS/4% formaldehyde and permeabilization with PBS/0.1% Triton X-100. Incubation with primary antibodies [1: 200 dilution in PBS/5% foetal bovine serum (FBS; Life Technologies)] and corresponding Alexa Fluor 488/568-conjugated secondary antibodies (Life Technologies; 1:400 dilution in PBS/5% FBS) was done at 4°C. Nuclear counterstaining was performed at room temperature with 10 µg/mL Hoechst 33342 (Life Technologies) in PBS/5% FBS. Coverslips were mounted in Vectashield mounting medium (Vector Laboratories, Burlingame, CA, USA). Images were acquired with a digital colour camera-equipped fluorescence microscope (Nikon Eclipse 80i; Nikon Instruments Europe, Amstelveen, the Netherlands). Storage and quantification of immunofluorescence signals was done using dedicated software [NIS Elements (Nikon Instruments Europe) and ImageJ (version 1.43; National Institutes of Health, Bethesda, MD, USA)]. Each immunostaining was performed on ≥3 independent aCMC cultures.

Western blotting

Cells were lysed in RIPA buffer [50 mM Tris–HCl (pH 8.0), 150 mM NaCl, 1% Triton X-100, 0.5% sodium deoxycholate, 0.1% sodium dodecyl sulfate supplemented with protease inhibitors (cOmplete, Mini Protease Inhibitor Cocktail Tablet; Roche Applied Science, Penzberg, Germany)]. Protein concentration was determined with the BCA Protein Assay Reagent (Thermo Fisher Scientific). Proteins were size-fractionated in NuPage Novex 12% Bis–Tris gels (Life Technologies) and transferred to Hybond polyvinylidene difluoride membranes (GE Healthcare, Diegem, Belgium) by wet electroblotting. After blocking for 1 h in Tris-based saline/0.1% Tween-20 (TBS-T)/5% bovine serum albumin (BSA; Sigma-Aldrich), membranes were incubated for 1 h with primary antibodies directed against green fluorescent protein (rabbit IgG; 1:1000; Life Technologies, A-11122) to detect eYFP or the CatCh~eYFP fusion protein or against glyceraldehyde 3-phosphate dehydrogenase (GAPDH; mouse IgG1, clone 6C5; 1:100 000; Merck Millipore, Billerica, MA, USA) as loading control. Next, blots were incubated with corresponding horseradish peroxidase-conjugated secondary antibodies (1:1000 in TBST/5% BSA; Santa Cruz Biotechnology, Dallas, TX, USA) again for 1 h. Blots were then immersed in ECL Prime Western blot detection reagent (GE Healthcare) and chemiluminescence was measured with the ChemiDoc XRS imaging system (Bio-Rad Laboratories, Veenendaal, the Netherlands).

Optical mapping

To analyse the electrophysiological effect of CatCh-generated photocurrents on aCMC cultures, cells were assayed by optical mapping on Day 7 or 8 of culture. Action potential (AP) propagation was visualized using the voltage-sensitive dye di-4-ANEPPS (Life Technologies). Cells were stimulated either electrically with an epoxy-coated bipolar platinum electrode with square suprathreshold electrical stimuli at 1–2 Hz or optically with light pulses from a 470 nm light-emitting diode (LED; SR-01-B0040 Rebel Star LED assembly; 70 Lm at 700 mA; Luxeonstar, Brantford, Ontario, Canada) mounted 10 mm below the centre of the wells of a 24-well cell-culture plate. A specialized stimulus generator (STG 2004) with corresponding software (MC Stimulus II; both from Multichannel Systems, Reutlingen, Germany) was used to perform both electrical and optical stimulation (see also Supplementary material online, *Figure S1*). Irradiance was measured using a PM100D optical power meter (Thorlabs, Munich, Germany) equipped with a S130C slim dual range sensor with the range set at 5 nW–5 mW and the wavelength set at 470 nm. Optical images were captured using a MiCAM ULTIMA-L imaging system (SciMedia, Costa Mesa, CA, USA). Optical pacing was performed by exposure for 10 ms to blue LED light at the maximal irradiance achievable with our setup (0.038 mW/mm^2). Strength–duration curves of optical pacing threshold were constructed by varying pulse duration (5–25 ms) and irradiance (0.0050–0.038 mW/mm^2). Reentry was induced by electrical burst pacing with a cycle length of 20–100 ms. After confirmation of the presence of reentrant arrhythmias, cultures

were exposed to blue LED light for 500 ms (at 0.038 mW/mm^2). Specialized software was used for data analysis and construction of activation maps (BrainVision Analyzer 1101; Brainvision, Tokyo, Japan). For baseline shift adjustment during blue LED light exposure, several filters were applied allowing data interpretation during the LED-on period (see Supplementary material online, *Figure S1*). The phase-space method was used to identify and track phase singularities (PSs) of spiral waves as described previously.[16] As measure of wavefront curvature, the straight distance between the spiral wave tip and the point of the first (or second) half winding of the wavefront was determined.[17] To this purpose, a tangent line was drawn along the wavefront in the direct vicinity of the PS (Supplementary material online, *Figure S3,* dashed white lines). Next, the length of the normal line from its intersection with the tangent line to its intersection with the wavefront at half of the spiral wave's full winding was measured (Supplementary material online, *Figure S3*).

MEA mapping

To provide additional mechanistic insight into CatCh-mediated effects on spiral waves and to avoid potential complexities associated with the combined application of light-activated potentiometric dyes and ion channels (see also Supplementary material online, *Figure S1*), MEA mapping of extracellular potentials was performed in parallel to optical mapping as a matching non-optical control.

For MEA mapping, aCMCs were cultured in fibronectin-coated MEA culture dishes containing 60 30 µm-diameter electrodes with an interelectrode spacing of 200 µm (Multi Channel Systems). Next, reentry was induced by electrical burst pacing as described earlier. During recording, cultures were exposed to blue LED light pulses (10 ms for optical pacing or 500 ms for reentry termination). Electrograms were analysed using MC-Rack software (Multi Channel Systems).[18]

Whole-cell patch-clamp recordings

Voltage-clamp recordings in single LV.CatCh∼eYFP↑-transduced aCMCs were carried out in parallel to optical mapping experiments. Transduced cells (identified by their green-yellow fluorescence) were exposed to 10 or 500 ms blue LED light pulses to study CatCh-mediated photocurrents, after reaching GΩ seal, establishing whole-cell configuration, and setting holding potential at −45 mV. Experiments were performed at 19–23°C using a MultiClamp 700B amplifier, a Digidata 1440A A/D converter, Clampex 10.3 software (all from Axon CNS, Molecular Devices, Sunnyvale, CA, USA), the STG 2004 pulse generator with corresponding computer software, and an Axiovert 35 inverted phase-contrast and fluorescence microscope (Carl Zeiss). Cells were bathed in an extracellular solution composed of (in mmol/L) 137 NaCl, 5 KCl, 1 $MgCl_2$, 1.8 $CaCl_2$, 10 HEPES, and 11 glucose (pH 7.4 adjusted with NaOH). Patch pipettes

manufactured from borosilicate glass with capillary 1.5 mm outer diameter and 1.17 mm inner diameter (Harvard Apparatus, Kent, UK) were pulled by a model P-30 vertical micropipette puller (Sutter Instrument Company, Novato, CA, USA). The internal pipette solution contained (in mmol/L) 20 NaCl, 120 KCl, 1 $MgCl_2$, 5 EGTA, and 10 HEPES (pH 7.4 adjusted with KOH). Pipettes showed a typical resistance of 2–3 MΩ and liquid junction potentials (~5 mV) were corrected. Data were digitized at 10 kHz, filtered at 10 kHz (4-pole Bessel low-pass filter, 24 dB/octave, −3 dB at cut off) and analysed off-line using pClamp 10 electrophysiology data acquisition and analysis software (Axon CNS, Molecular Devices).

Statistical analysis

Statistical analyses were performed using SPSS11.0 for Windows (SPSS, Chicago, IL, USA). The Mann–Whitney *U* test or the Wilcoxon signed rank test was used for comparison between groups as indicated. Data were expressed as mean ± standard deviation (SD) for a number (*n*) of observations. Differences were considered statistically significant at $P < 0.05$.

Results

Characterization of 2D AF model

Immunocytological analysis at Day 8 showed that 100% of the α-actinin$^+$ cells in monolayer cultures of neonatal rat atrial cells were positive for MLC2a, i.e. no MLC2a$^-$/α-actinin$^+$ cells were detected, confirming that all cardiomyocytes in these cultures were of atrial origin (*Figure 1A*). Cultures contained 18.3 ± 4.8% fibroblasts as judged by collagen type 1 immunostaining (*Figure 1B*). At Day 8 of culture, cells showed abundant Cx43 expression at intercellular junctions (*Figure 1C*) forming a dense 'syncytial' monolayer (*Figure 1D*), which could be assessed for conduction patterns by optical mapping and by MEA analysis. Typically, no spontaneous activity was observed in the atrial cell cultures. Upon 1 Hz electrical stimulation cultures showed 1:1 uniform convex activation originating from the bipolar pacing electrode, while no PSs were observed (*Figure 1E* and *G*), resembling normal atrial activation as occurs during sinus rhythm. However, after burst pacing, multiple spiral wave reentry circuits and corresponding PSs arose maintaining high-frequency activation (mean 13.8 ± 7.0 Hz) independent of any subsequent electrical stimulation (*Figure 1F* and *H*), resembling activation patterns found in AF.

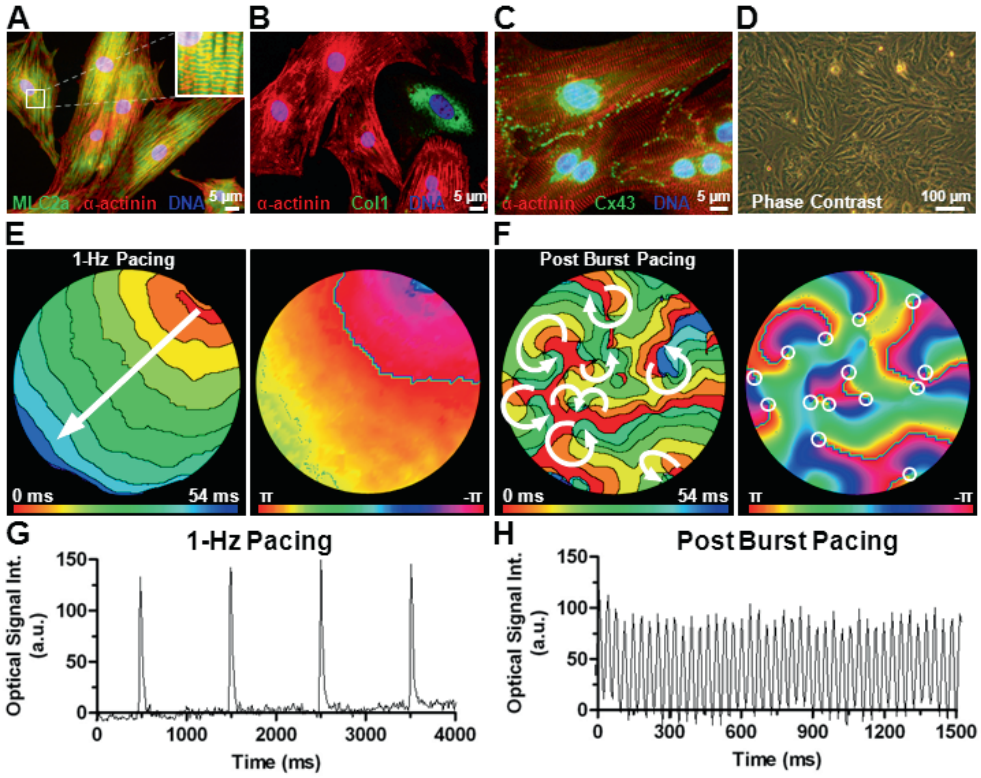

Figure 1. Characterization of 2D AF model. Typical examples of immunocytological double stainings for (*A*) MLC2a (aCMCs, green) and α-actinin (cardiomyocytes, red), (*B*) α-actinin (cardiomyocytes, red) and collagen type 1 (Col1; fibroblasts, green), and (*C*) α-actinin (cardiomyocytes, red) and Cx43 (gap junctions, green) in atrial cell cultures. The white inset in *A* (top right) shows a magnification of the boxed area (left). (*D*) Phase contrast image of a confluent atrial cell monolayer. (*E*) Typical activation map (6 ms isochrone spacing) and corresponding phase map of an atrial culture during 1 Hz electrical pacing, showing uniform convex propagation originating from the electrode (in the direction of the white arrow; left panel) and absence of PSs (right panel). (*F*) Typical activation map (6 ms isochrone spacing) and corresponding phase map of an atrial culture after electrical burst pacing. Multiple reentrant circuits are evident in the activation map, following the directions of the white arrows. The phase map shows multiple PSs indicated by white circles. Typical spatially filtered optical (i.e. di-4-ANEPPS-derived) signal traces in an atrial culture (*G*) during 1 Hz pacing and (*H*) after fibrillation is established by electrical burst pacing. a.u., arbitrary units.

Confirmation of functional CatCh expression

Atrial cell cultures were transduced with either the lentiviral vector LV.CatCh~eYFP↑ encoding a fusion protein between CatCh and eYFP, or the eYFP-encoding lentiviral vector LV.eYFP↑ as a control, to study the effects of CatCh activation on spiral waves (for vector maps, see *Figure 2A*). Because transgene expression is driven by a striated muscle-specific promoter, lentiviral vector-transduced atrial cultures showed eYFP signals almost exclusively in the α-actinin$^+$ cells (100 ± 38.6 vs. 8.7. ± 1.7 arbitrary units in non-myocytes and 100 ± 37.0 vs. 4.2 ± 1.6 arbitrary units in non-myocytes for the LV.eYFP↑- and LV.CatCh~eYFP↑-transduced cultures, respectively; $P <$

0.05). As expected, in the LV.eYFP↑-transduced aCMCs, eYFP localized to the cytoplasm, while in the LV.CatCh∼eYFP↑-modified cells, eYFP fluorescence was membrane-associated (*Figure 2B–D*). Western blot analysis confirmed eYFP expression in atrial cell cultures after transduction with both LV.eYFP↑ and LV.CatCh∼eYFP↑, showing immunoreactive protein species of ∼27 kDa (the predicted molecular weight of eYFP) and of around 60 kDa (due to fusion of CatCh to the N terminus of eYFP), respectively (*Figure 2E*). Optical and MEA mapping experiments showed that APs could be elicited by optical pacing through exposure to 10 ms light pulses (at 0.038 mW/mm^2) in LV.CatCh∼eYFP↑- but not in LV.eYFP↑-transduced cultures (see also Supplementary material online, *Figure S2* for a strength–duration analysis of the pacing threshold in LV.CatCh∼eYFP↑-transduced cultures), while both culture types could be paced electrically (*Figure* 3*A* and *B*; $n = 12$ and $n = 9$, respectively). The maximum change in fluorescence intensity occurred within 12.0 ± 8.5 ms ($n = 5$) throughout the culture (*Figure 3C*), indicating synchronous depolarization of the monolayer by CatCh activation. The functionality of the generated photocurrent was further confirmed in patch-clamp experiments on single aCMCs (*Figure* 3*D*), which revealed inward currents with a peak current density of 5.31 ± 1.13 pA/pF upon exposure to 10 ms blue light pulses ($n = 6$).

Light-induced spiral wave termination

Exposure to prolonged light pulses (500 ms at 0.038 mW/mm^2), producing a sustained current with a peak density of 12.01 ± 2.54 pA/pF in single aCMCs ($n = 6$; *Figure 3D*), led to spiral wave termination in all of the LV.CatCh∼eYFP↑- (31 out of 31), but none of the LV.eYFP↑-transduced (0 out of 11) cultures, as judged by optical mapping analyses and confirmed by MEA recordings (*Figure 4A–F*). Importantly, LV.CatCh∼eYFP↑-transduced cultures that had been subjected to repeated optogenetic spiral wave termination displayed normal uniform conduction upon subsequent electrical activation implying retained excitability (*Figure 4E*).

No significant persisting electrophysiological or pro-arrhythmic changes were observed in LV.CatCh.eYFP↑-transduced cultures following prolonged exposure (i.e. 500 ms) to blue light (see Supplementary material online, *Figure S4*). Also, contractility, as judged by phase-contrast microscopy, was retained after expression of CatCh∼eYFP and its subsequent activation by a 500 ms blue light pulse. During exposure to a 500 ms light pulse, reentry was terminated within 163.1 ± 105.8 ms (range 36–444 ms, $n = 22$) suggesting that reentry could be terminated using pulses shorter than 500 ms. Hence, to find the pulse duration necessary for termination, we induced reentry in LV.CatCh.eYFP↑-transduced cultures and attempted spiral wave termination by exposure to subsequent blue light pulses of 10, 20, 50, 100, 200, and 500 ms at 0.038 mW/mm^2. This showed that the average pulse duration necessary for arrhythmia termination was 133.3 ± 180.7 ms ($n = 6$).

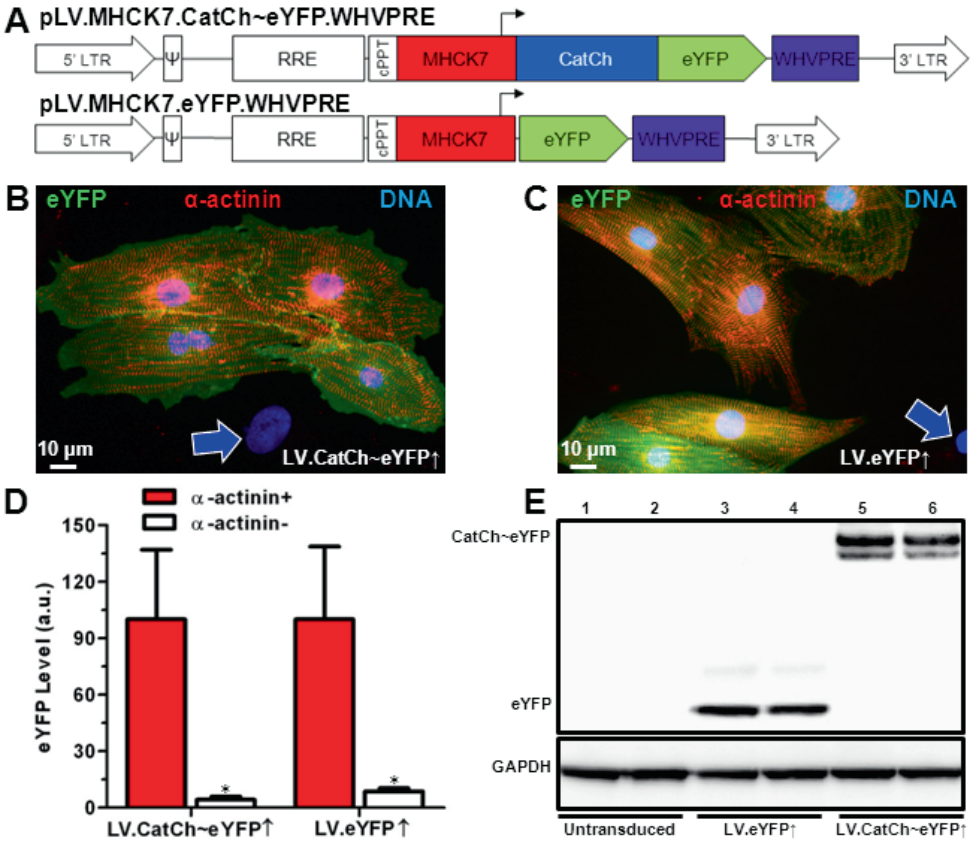

Figure 2. Immunocytological and western blot confirmation of forced CatCh expression. (*A*) Structure of the lentiviral vector DNA in plasmids pLV.MHCK7.CatCh~eYFP.WHVPRE (for generating LV.CatCh~eYFP↑) and pLV.MHCK7.eYFP.WHVPRE (to produce LV.eYFP↑). 5′ LTR: chimeric 5′ long terminal repeat containing enhancer and promoter elements of the human cytomegalovirus *immediate-early* gene and the human immunodeficiency virus type 1 (HIV1) R and U5 regions. Ψ: HIV1 packaging signal. RRE: HIV1 Rev-responsive element. cPPT: HIV1 central polypurine tract and termination site. MHCK7: chimeric striated muscle-specific promoter.[13] CatCh: coding sequence of an ultra-light-sensitive and highly Ca^{2+}-permeable mutant of the *Chlamydomonas reinhardtii* chlamyopsin 4 light-gated ion channel, also known as ChR2.[10] eYFP: *Aequorea victoria* enhanced yellow fluorescent protein-coding sequence. WHVPRE: woodchuck hepatitis virus posttranscriptional regulatory element. 3′ LTR: wild-type 3′ HIV1 LTR. (*B* and *C*) Immunocytological staining of (*B*) LV.CatCh~eYFP↑- and (*C*) LV.eYFP↑-transduced atrial cultures for α-actinin (red; cardiomyocyte marker), showing membrane-associated and cytoplasmic eYFP signals (green), respectively. Blue arrows indicate nuclei of $eYFP^{-}$/$\alpha\text{-actinin}^{-}$ cells (mainly cardiac fibroblasts). (*D*) Quantification of the eYFP signal in $\alpha\text{-actinin}^{+}$ (red bars) and $\alpha\text{-actinin}^{-}$ (white bars) cells in atrial cultures after transduction with LV.CatCh~eYFP↑ or with LV.eYFP↑. (*E*) Western blot analysis of eYFP/CatCh~eYFP levels in untransduced (lanes 1 and 2) atrial cultures and cultures transduced with LV.eYFP↑ (lanes 3 and 4) or with LV.CatCh~eYFP↑ (lanes 5 and 6) using glyceraldehyde 3-phosphate dehydrogenase (GAPDH) as loading control. $^{*}P < 0.05$ vs. $\alpha\text{-actinin}^{+}$ using the Mann–Whitney *U* test. a.u., arbitrary units.

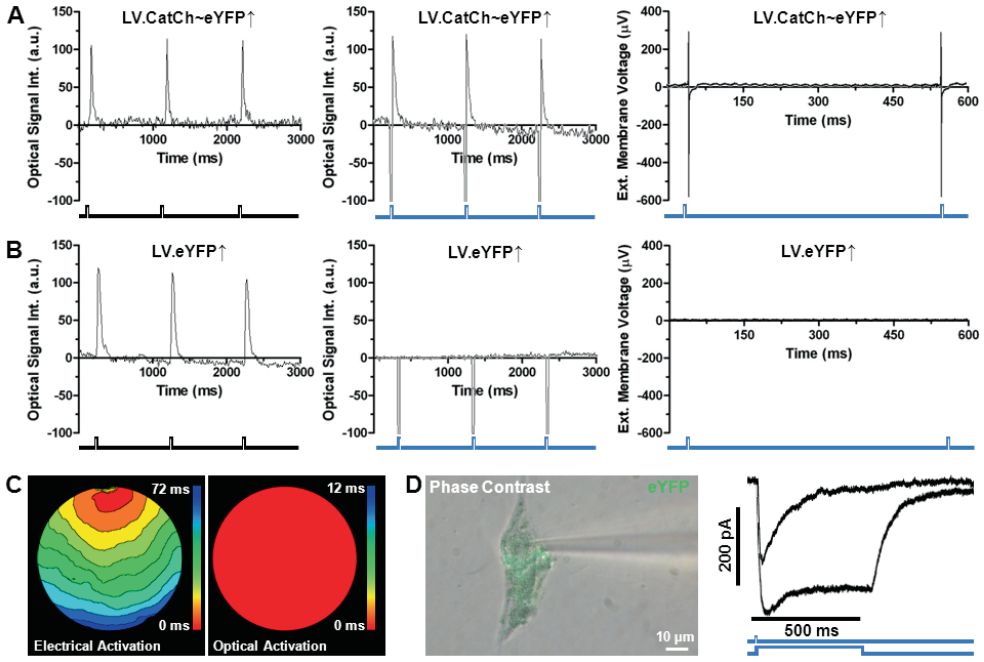

Figure 3. Confirmation of functional CatCh expression. (*A* and *B*) Typical optical signal traces (left and middle panels) and MEA recordings (right panels) in aCMC cultures transduced with (*A*) LV.CatCh~eYFP↑ or with (*B*) LV.eYFP↑ during 1 Hz electrical activation (left panels) or exposure to 10 ms blue light pulses at 1 Hz (middle panels) and 2 Hz (right panels). (*C*) Activation map of an LV.CatCh~eYFP↑-transduced atrial culture during 1 Hz electrical pacing (left) and exposure to a 10 ms blue light pulse of 1 Hz (right). (*D*) Typical example of a *CatCh~eYFP*-expressing aCMC used for patch-clamping (left) and two superimposed records of whole-cell inward currents from the same aCMC evoked at a holding potential of −45 mV by a 10 and 500 ms blue light pulse of equal intensity (see bottom traces) (right). As expected, non-transduced aCMCs did not show light-dependent currents. a.u., arbitrary units.

Next, we investigated the anti-arrhythmic mechanism underlying arrhythmia termination by CatCh activation. During reentry, a gradient in conduction velocity and AP amplitude was observed. Both parameters decreased near the spiral wave core (*Figure 5A*) while wavefront curvature was significantly higher near the core than in the periphery (the second vs. the doubled first half winding distance of the wavefront was 7.2 ± 1.9 vs. 4.1 ± 1.1 mm; $P < 0.05$, $n = 6$) (*Figure 5B*).

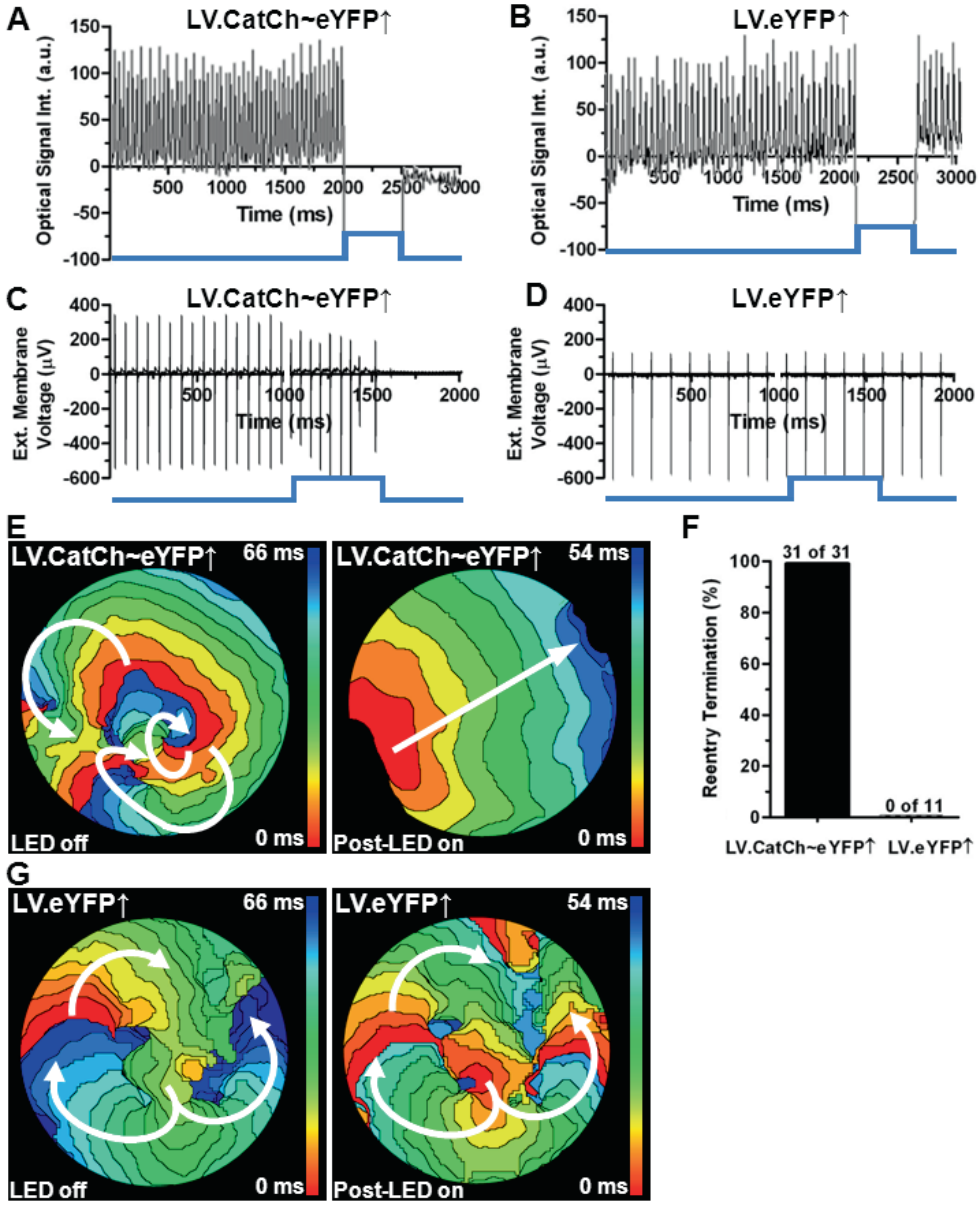

Figure 4. Effective light-induced spiral wave termination by CatCh expression. Typical signal traces in reentrant tachyarrhythmic atrial cultures transduced with (*A* and *C*) LV.CatCh~eYFP↑ or with (*B* and *D*) LV.eYFP↑ during (*A* and *B*) optical mapping or (*C* and *D*) MEA recordings, showing termination of tachyarrhythmic activity after exposure to blue light (500 ms duration) in LV.CatCh~eYFP↑ cultures only. Typical activation map of (*E*) LV.CatCh~eYFP↑- and (*G*) LV.eYFP↑-transduced atrial cultures before (left panel) and after (right panel) exposure to a 500 ms blue light pulse, showing light-induced termination of reentrant activity. (*F*) Quantification of the success rate of light-induced spiral wave termination in LV.CatCh~eYFP↑- and LV.eYFP↑-transduced cultures. a.u., arbitrary units.

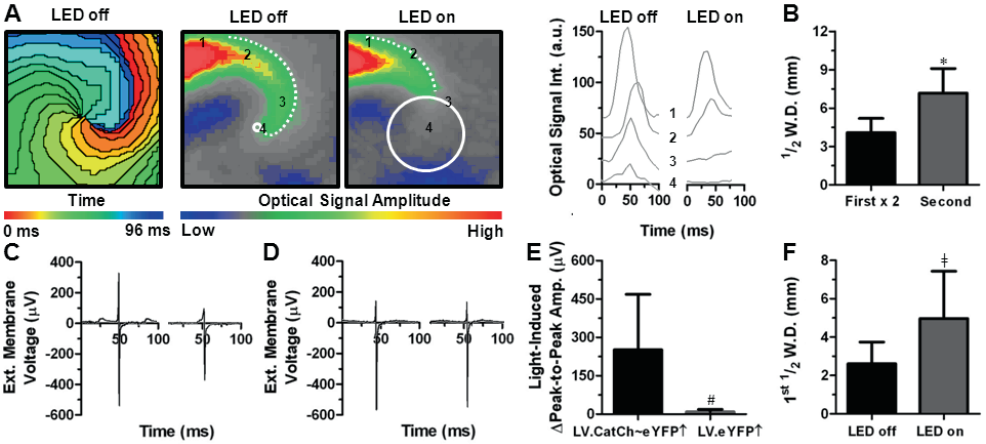

Figure 5. Light-induced increase in functional core size. (*A*) Activation map (left panel) and snapshots (two middle panels) after spatial and high-pass filtering of optical signals of an LV.CatCh~eYFP↑-transduced atrial culture before and during exposure to a 500 ms blue light pulse (6 ms isochrone spacing). The optical signal traces (non-high-pass-filtered) are shown on the right. Numbers 1–4 correspond to the positions in the snapshots. White circles indicate estimated functional core sizes. (*B*) Quantification of the doubled first half winding distance (½ W.D.) of the wavefront and the second half winding distance as a measure of wavefront curvature during reentry in LV.CatCh~eYFP↑-transduced atrial cultures. (*C*) Typical MEA recordings of LV.CatCh~eYFP↑- or (*D*) LV.eYFP↑-transduced atrial cultures during reentrant activity before (left) and at the beginning (right) of a 500 ms blue light pulse. (*E*) Quantification of MEA peak-to-peak amplitude changes upon exposure to blue light in LV.CatCh~eYFP↑- and LV.eYFP↑-transduced cultures. (*F*) Quantification of the first half-winding distance in LV.CatCh~eYFP↑-transduced cultures prior to (LED off) and during (LED on) exposure to a 500 ms blue light pulse as a measure of wavefront curvature. $^{*}P < 0.05$ vs. doubled first half-winding distance using a Wilcoxon signed rank test. $^{\#}P < 0.05$ vs. LV.CatCh~eYFP↑-transduced cultures using a Mann–Whitney *U* test. $^{\ddagger}P < 0.05$ vs. LED on using a Wilcoxon signed rank test. a.u., arbitrary units.

Depolarization by activation of CatCh led to a reduction in overall excitability. The reduction in excitability caused by light-induced depolarization was confirmed by MEA mapping showing a strong decrease in peak-to-peak amplitude [Δpeak-to-peak amplitude 251.3 ± 217.1 µV in LV.CatCh~eYFP↑-transduced cultures ($n = 6$) vs. 9.2 ± 9.5 µV in LV.eYFP↑-transduced cultures ($n = 5$) (*Figure 5C* and *E*], likely attributable to inactivation of the fast Na^+ current. As a consequence, the critical wavefront curvature (the curvature at which the conduction velocity becomes zero, i.e. the curvature near the spiral wave core) was decreased (first half-winding distance was 2.6 ± 1.1 before light exposure vs. 5.0 ± 2.5 mm during light exposure, $n = 6$) (*Figure 5F* and Supplementary material online, *Figure S3*). Hence, during light exposure, the critical wavefront curvature is reached at a more peripheral point in the wavefront compared with the point of PS (i.e. the point of critical wavefront curvature) before light exposure. Since the source–sink relationship for impulse propagation in cardiac tissue does not allow wavefront curvature to exceed a critical value, spiral wave core size increased after the decrease in excitability during light exposure. This was evinced by a reduction in AP amplitude and inhibition of excitation near the functional core (*Figure 5A*).

As a consequence of the lowered critical curvature, culture-wide expansion of the PS trajectory around the growing functional core occurred, which increased the probability of critical collisions of PSs with culture boundaries (*Figure 6A* and Supplementary material online, *Movie S1*) or with PSs of opposite chirality (*Figure 6B* and Supplementary material online, *Movie S2*), ultimately causing spiral wave termination.

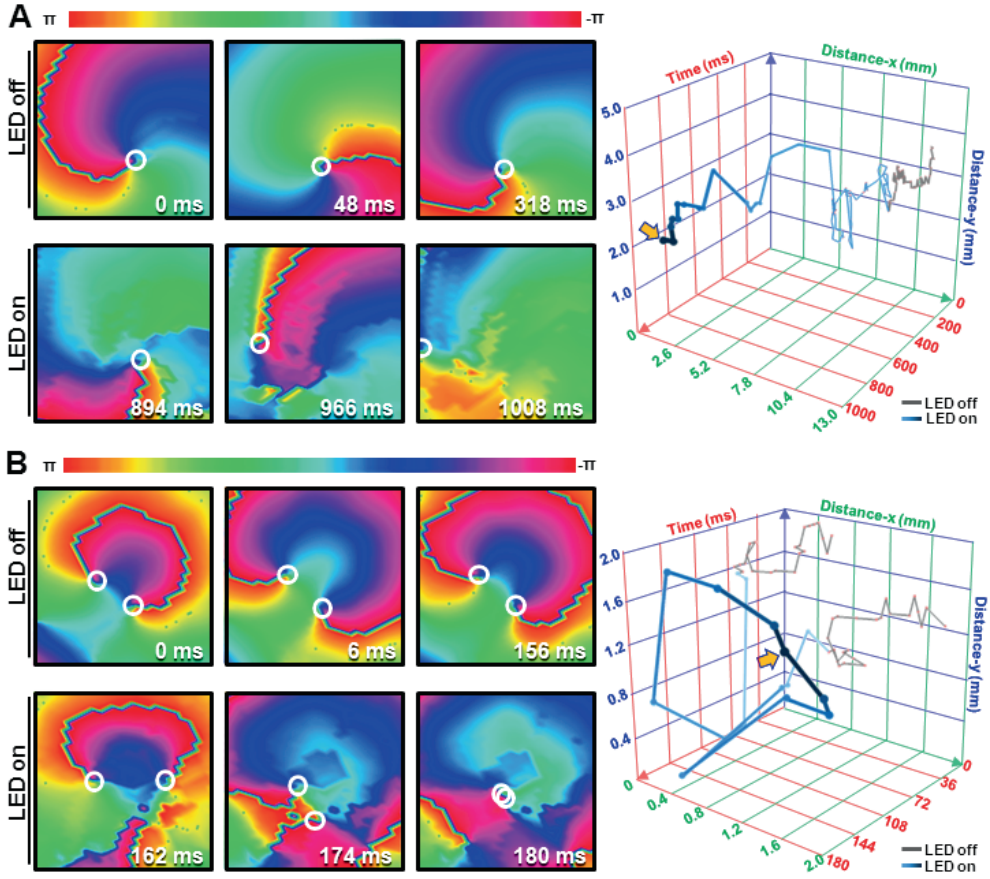

Figure 6. Light-induced alteration of PS trajectory and arrhythmia termination. Typical phase map sequence of an LV.CatCh~eYFP↑-transduced atrial culture showing spiral wave phase progression before (upper sequences) and during (lower sequences) exposure to blue light leading to spiral wave termination by (*A*) PS–boundary collision and (*B*) PS–PS collision. White circles indicate PS positions. 3D graphs show the PS positions before (grey) and during (blue gradient) exposure to blue light, exemplifying PS drift leading to wave termination (yellow arrow).

Discussion

The key findings of this study are the following: first, neonatal rat aCMCs can be endowed with functional light-gated cation channels (i.e. CatCh) by lentiviral transduction without evident alterations in the characteristics of the AP or calcium transient. Secondly, activation of these channels by brief light pulses (10 ms/470 nm) provides a depolarizing current strong enough to serve as suprathreshold stimulus for instant and synchronous electrical activation of CatCh-expressing cardiomyocytes in atrial monolayer cultures. Thirdly, in such monolayers, stable rotors with PSs rotating around functional cores and maintaining fibrillatory activation can be terminated effectively and repeatedly by prolonged activation of CatCh (500 ms light exposure). Fourthly, mechanistically, prolonged CatCh activation reduces overall excitability of the fibrillating monolayers, followed by an increase in functional core size, resulting in PS drift, which ultimately leads to termination of the spiral wave arrhythmias. Finally, this is the first study to show that optogenetic engineering of neonatal rat aCMCs, by means of forced CatCh expression and subsequent photoactivation, allows fibrillating aCMC monolayers to generate themselves the electrical current needed for defibrillation. This proof-of-concept may give a strong impetus towards the design of shockless treatment strategies for AF.

Optogenetic control of cardiac excitability

In the past, most studies that aimed to unravel the mechanisms underlying cardiac arrhythmias and to identify new anti-arrhythmic targets relied exclusively on the use of pharmacological and/or electrical interventions to modulate electrophysiological processes in cardiomyocytes, like de- and hyperpolarization.[12,16,18] More recently, genetic interventions including site-directed mutagenesis, gene knockdown/knockout and forced (trans)gene expression have been added to the repertoire of techniques to modulate cardiac ion channel activity and excitability in a more refined manner.[11] Nevertheless, even today's most sophisticated genetic interventions allow for only modest spatiotemporal, as well as, quantitative control of the target's functionality. Such constraints hamper further progress in our mechanistic understanding and treatment of cardiac arrhythmias. Optogenetic engineering, however, allows modulation of cellular electrophysiological properties with superb spatiotemporal and quantitative control in a non-voltage-gated fashion by combining the favourable properties of photoactivatable ion channels and light.[6] As a result, optogenetics has become an indispensable tool in neuroscience to modulate the activity of neurons by light and thereby study the functional roles of specific neural pathways in the brain.[6]

More recently, optogenetics was introduced in the field of cardiovascular research by showing that channelrhodopsin-2 (ChR2)-expressing cardiomyocytes, either cultured *in vitro* or present in the intact heart, could be electrically excited by brief light pulses without obvious adverse

effects on cardiac function.[7–9] These pulses caused depolarization of cardiomyocytes at the site of illumination, thereby triggering APs that were rapidly propagated across the cardiac tissue via gap junctions and merged into a spread of uniform electrical activation. Prolonged activation of light-gated cation channels in cardiomyocytes led to sustained depolarization of all cardiomyocytes without causing noticeable adverse effects.[7] However, thus far, the potential of optogenetics to counteract cardiac tachyarrhythmias has not been investigated.

Optogenetic termination of spiral waves

Based on current evidence, reentrant spiral waves play a major role in the maintenance of fibrillation in both atria and ventricles.[19] Hence, most strategies aiming to prevent or terminate AF involve the inhibition of reentry formation and the elimination of existing reentrant circuits, respectively. Previous studies have shown that during reentry, conduction velocity and excitability gradually increase from the rotor core towards the periphery. Paramount to the establishment of these gradients seem to be the inward rectifier K^+ current (I_{K1}) and the fast Na^+ current (I_{Na}), of which the amplitudes decrease towards the rotor core. The interplay between I_{K1} and I_{Na} determines reentry frequency and rotor stability as a decrease of either current slows and destabilizes the rotor, possibly leading to spiral wave termination.[16,20,21] The present study is consistent with this concept, as a light-induced decrease in overall excitability increased the functional core size and terminated reentry. Due to the existing gradient in excitability, decreasing overall excitability will first prevent excitation near the core leading to its expansion thereby causing PS drift from a relatively stable position. Consequently, the chance for PSs to collide with each other or with physical boundaries will increase. Following light-triggered annihilation of all PSs in a culture, as found in our experiments, no spiral waves are generated anymore, allowing reestablishment of a regular cardiac activation pattern. Still, as optogenetic defibrillation is a new field of research, various aspects of this method need to be investigated in further detail in order to fully appraise its value as a research tool and to gain more insight into its therapeutic potential.

Potential advantages over established defibrillation strategies

While pharmacological blockade of I_{K1} and I_{Na} are well-accepted strategies to terminate reentry, they are associated with proarrhythmia, since the resulting chronic slowing of repolarization and conduction promote afterdepolarizations and reentry, respectively.[16,22] Optogenetic therapy would, however, decrease excitability only during photostimulation, leaving important electrophysiological parameters unaltered after spiral wave termination.

Several advantages of optogenetic therapy over electrical cardiac therapy have been previously postulated in the light of cardiac pacing, including a higher level of spatial control[7,8] and, more importantly, higher energy efficiency resulting in less tissue damage. For CatCh, the

enhanced energy efficiency might be even more pronounced than for earlier ChR2 variants due to its improved light sensitivity. While optical pacing might prove an interesting option for treatment of bradyarrhythmias, energy efficiency could be of even greater importance when trying to normalize heart rhythm during tachyarrhythmia. The possible applicability of optogenetics in the field of tachyarrhythmias was already hinted at in a study showing the ability to cause light-induced conduction block by overexpression of the hyperpolarizing light-sensitive Cl^- channel NpHR in zebrafish cardiomyocytes.[7] Moreover, using ChR2(H134R), Bruegmann *et al.*[8] showed that through a depolarizing photocurrent spontaneous beating of embryonic stem cell-derived cardiomyocytes could be depressed, most likely as a result of fast Na^+ channel inactivation upon prolonged local illumination. In the present study, the possibility to optogenetically suppress cardiac excitability was confirmed by prolonged light exposure of aCMCs expressing the Ca^{2+}-permeable and ultra-light-sensitive ChR2 mutant CatCh. The CatCh-dependent photocurrent was used to show that uniform light-induced depolarization can terminate spiral wave reentry, exemplifying the possibility to broaden the field of optogenetic control of myocardial function towards arrhythmia termination. In sharp contrast, traditional defibrillation is based on the delivery of high-energy electrical shocks to cause uniform depolarization. The use of high-energy electrical shocks is associated with severe discomfort in patients as well as tissue damage, increasing with stimulus strength and duration. A major improvement in electrical defibrillation has been the introduction of the biphasic waveform[23] and further technical refinements like multistage electrotherapy[24] are arising. Still, stimulus duration in traditional defibrillation must be confined to several milliseconds, whereas the optogenetic approach might enable the use of longer stimuli, such as applied in this study, without inducing tissue damage.

During traditional electrical defibrillation, reentry can be re-initiated at critical points in local electrical field strength, when shock strength is below the upper limit of vulnerability or when the shock causes the occurrence of virtual electrodes from which new fibrillatory waves can emanate.[5,25–27] Since optogenetic defibrillation, as presented in this study, does not use an electric field to induce depolarization, it should not result in re-initiation of fibrillation by the formation of virtual electrodes. Under conditions of homogeneous transduction and illumination also re-initiation as a consequence of aforementioned critical points may be prevented by optogenetic arrhythmia termination. Concordantly, after light-induced spiral wave termination, no proarrhythmic reexcitations were found in our model. Thus, as shown in the present study, optogenetic therapy to control cardiac function and to terminate arrhythmias might provide several advantages over the traditional means of treating heart rhythm disorders.

Translational considerations and study limitations

This study shows that the endogenous electrochemical gradients present in cardiac tissue can be exploited for defibrillation by optogenetics, as an alternative to the external electrical current applied to interrupt reentrant circuits during conventional electrical defibrillation.[5] However, we acknowledge that translating this principle to the *in vivo* situation comes with some hurdles that need to be overcome before considering any clinical applications.

First, in the present study, a 2D model of AF was used to demonstrate proof-of-principle for the optogenetic termination of fibrillatory conduction. This *in vitro* model lacks the complexity found in the intact 3D atrium and thus does not suffer from factors such as a low transduction efficiency of the target cell population and poor light penetration into the target tissue that might limit the effectiveness of optogenetic arrhythmia termination *in vivo*. Moreover, as we found termination of reentry by light to depend on the collision of PSs with boundaries or with PSs of opposite chirality, at least an area including the PS and its nearest physical boundary or a counteracting PS has to be illuminated for successful arrhythmia termination. However, because in our model the position of the PSs causing reentrant activation cannot be predetermined and their trajectories cannot be controlled, homogeneous illumination of the entire aCMC cultures is required for consistent reentry termination by light. Still, earlier work in the field of ventricular fibrillation has shown that effective defibrillation does not require every cell in the myocardium to be depolarized,[5] hinting at the possibility that successful defibrillation may also be achieved in the case of incomplete light penetration and/or patchy transgene expression. This might even be more pronounced in AF, as rotors or drivers of AF usually localize to specific areas of the atrium such as the direct surroundings of pulmonary vein ostea. Hence, future studies testing the possibility of AF termination using local instead of global cation channel activation may provide an important next step in the realization of shockfree defibrillation *in vivo*.

Nevertheless, in tackling the possibility of insufficient light penetration *in vivo*, it may be critical to expand the optogenetic toolbox with improved/mutated light-gated cation channels displaying greater light sensitivity or increased ion conductance. In addition, due to the absorption of especially short-wavelength visible light by tissue constituents like blood, it might be of interest to look into (optogenetic) tools that are excited by light of higher wavelength (i.e. near-infrared) or by other energy sources (radio waves/ultrasound) and therefore allow deeper tissue penetration. These improvements are likely to arise in the near future through the ongoing research and advances in (opto)genetic technology.[6,28]

Secondly, it should be noted that the physical boundaries of culture dishes (necessary for extinguishing PSs by collision, in addition to the collision to PSs of opposite chirality) differ from the anatomical boundaries in the intact atrium. Nonetheless, in several clinical studies, PS–boundary collisions have been identified as a mechanism of rotor termination in both

atrial and ventricular fibrillation.[29,30] Hence, while in the intact atrium, the likelihood of a PS meeting a PS of opposite chirality may be diminished compared with that in our 2D model, light-induced rotor termination *in vivo* might be facilitated by the numerous anatomical boundaries contained within the atrium, such as the many walls of the microvasculature, the mitral/tricuspid valve rings, the ostea of the pulmonary veins, and the epi- and endocardium.

Thirdly, in the present study, transgene expression was achieved by lentiviral vector-based gene transfer. Although lentiviral vectors are very efficient in inducing stable transgene expression *in vitro*, they are of limited use for *in vivo* cardiac gene therapy mainly because of their poor dissemination through myocardial tissue and their potential to cause insertional oncogenesis. These hurdles may be overcome by using adeno-associated virus (AAV) vectors for *in vivo channelrhodopsin* gene delivery to the heart as these vectors (i) can mediate long-term transgene expression in post-mitotic cells including cardiomyocytes without the need to integrate their DNA into the target cell genome, (ii) do not contain viral genes encoding potentially cytotoxic and/or immunogenic proteins, (iii) readily spread through myocardial tissue, and (iv) are well known for their excellent *in vivo* safety. The utility of AAV vectors for *in vivo* gene transfer to the human heart has been illustrated by a recent clinical study in which heart failure patients received AAV vector particles encoding sarco/endoplasmic reticulum Ca^{2+}-ATPase 2a,[31] paving the way for the clinical application of optogenetic and other gene-based therapies in the field of cardiology.

Finally, also the delivery method of the necessary light (or any other excitatory energy source) *in vivo* needs to be perfected. In the field of neurology, solutions to this problem have already been postulated, and lie in the use of, for example, fiberoptics.[32,33] Hence, the future might hold painfree implantable cardioverter defibrillator device therapy for AF, based on optogenetics and fibreoptic delivery of light, instead of electrical shocks applied via platinum leads, in specific areas of the atrial myocardium.

Without the intention to detract from this prospect, it should be noted that the conclusions drawn from the present study are only conceptual in relation to human AF and therefore cannot be readily extrapolated to the clinical setting. Hence, there is still a considerable amount of work to be done before optogenetic therapy (or any other therapy exploiting the electrochemical gradients that are endogenously present in myocardial tissue) becomes a realistic treatment option for patients with cardiac rhythm disorders.

Conclusions

In summary, forced expression of the light-gated cation channel CatCh in aCMCs allows for effective and repeated termination of reentrant conduction by photocurrent-induced functional core expansion. These results indicate that optogenetic control of cardiac electrical function could serve as a novel anti-arrhythmic strategy, in which the arrhythmogenic substrate

itself provides the defibrillating current. This may trigger the exploration of a previously uninvestigated principle to develop safe and effective new therapies for cardiac arrhythmias.

Funding

This work was supported by the Dutch Heart Foundation [E. Dekker grant (2012/T023 to B.O.B.)] and the Netherlands Organization for Scientific Research [Mosaic grant (017007064 to M.C.E.)]. D.A.P. is a recipient of a Vidi grant (91714336) of the Netherlands Organization for Scientific Research.

Acknowledgements

We thank Karl Deisseroth and Charu Ramakrishnan (Stanford University, Stanford, CA, USA) for providing the lentiviral vector shuttle plasmid pLenti-CaMKIIa-hChR2(L132C)-EYFP-WPRE, Ivan Kazbanov (Ghent University, Ghent, Belgium) for writing analysis software, and Huybert van der Stadt for excellent technical support.

Conflict of interest: none declared.

References

1. Lip GY, Tse HF, Lane DA. Atrial fibrillation. *Lancet* 2012;379:648-661.
2. Iwasaki YK, Nishida K, Kato T, Nattel S. Atrial fibrillation pathophysiology: implications for management. *Circulation* 2011;124:2264-2274.
3. Schotten U, Verheule S, Kirchhof P, Goette A. Pathophysiological mechanisms of atrial fibrillation: a translational appraisal. *Physiol Rev* 2011;91:265-325.
4. Wellens HJ, Lau CP, Luderitz B, Akhtar M, Waldo AL, Camm AJ, Timmermans C, Tse HF, Jung W, Jordaens L, Ayers G. Atrioverter: an implantable device for the treatment of atrial fibrillation. *Circulation* 1998;98:1651-1656.
5. Dosdall DJ, Fast VG, Ideker RE. Mechanisms of defibrillation. *Annu Rev Biomed Eng* 2010;12:233-258.
6. Deisseroth K. Optogenetics. *Nat Methods* 2011;8:26-29.
7. Arrenberg AB, Stainier DY, Baier H, Huisken J. Optogenetic control of cardiac function. *Science* 2010;330:971-974.
8. Bruegmann T, Malan D, Hesse M, Beiert T, Fuegemann CJ, Fleischmann BK, Sasse P. Optogenetic control of heart muscle in vitro and in vivo. *Nat Methods* 2010;7:897-900.
9. Jia Z, Valiunas V, Lu Z, Bien H, Liu H, Wang HZ, Rosati B, Brink PR, Cohen IS. Stimulating cardiac muscle by light: cardiac optogenetics by cell delivery. *Circ Arrhythm Electrophysiol* 2011;4:753-760.
10. Kleinlogel S, Feldbauer K, Dempski RE, Fotis H, Wood PG, Bamann C, Bamberg E. Ultra light-sensitive and fast neuronal activation with the Ca(2)+-permeable channelrhodopsin CatCh. *Nat Neurosci* 2011;14:513-518.
11. Bingen BO, Neshati Z, Askar SF, Kazbanov IV, Ypey DL, Panfilov AV, Schalij MJ, de Vries AA, Pijnappels DA. Atrium-Specific Kir3.x Determines Inducibility, Dynamics and Termination of Fibrillation by Regulating Restitution-Driven Alternans. *Circulation* 2013;128:2732-2744.
12. Askar SF, Ramkisoensing AA, Schalij MJ, Bingen BO, Swildens J, van der Laarse A, de Vries AA, Ypey DL, Pijnappels DA. Antiproliferative treatment of myofibroblasts prevents arrhythmias in vitro by limiting myofibroblast-induced depolarization. *Cardiovasc Res* 2011;90:295-304.
13. Salva MZ, Himeda CL, Tai PW, Nishiuchi E, Gregorevic P, Allen JM, Finn EE, Meuse L. Design of tissue-specific regulatory cassettes for high-level rAAV-mediated expression in skeletal and cardiac muscle. *Mol Ther* 2007;15:320-329.
14. Goncalves MA, Janssen JM, Nguyen QG, Athanasopoulos T, Hauschka SD, Dickson G, de Vries AA. Transcription factor rational design improves directed differentiation of human mesenchymal stem cells into skeletal myocytes. *Mol Ther* 2011;19:1331-1341.
15. Kubalak SW, Miller-Hance WC, O'Brien TX, Dyson E, Chien KR. Chamber specification of atrial myosin light chain-2 expression precedes septation during murine cardiogenesis. *J Biol Chem* 1994;269:16961-16970.
16. Bingen BO, Askar SF, Schalij MJ, Kazbanov IV, Ypey DL, Panfilov AV, Pijnappels DA. Prolongation of minimal action potential duration in sustained fibrillation decreases complexity by transient destabilization. *Cardiovasc Res* 2013;97:161-170.
17. Hou L, Deo M, Furspan P, Pandit SV, Mironov S, Auerbach DS, Gong Q, Zhou Z, Berenfeld O, Jalife J. A major role for HERG in determining frequency of reentry in neonatal rat ventricular myocyte monolayer. *Circ Res*. 2010;107:1503-1511.
18. Pijnappels DA, Schalij MJ, Ramkisoensing AA, van TJ, de Vries AA, van der Laarse A, Ypey DL, Atsma DE. Forced alignment of mesenchymal stem cells undergoing cardiomyogenic differentiation affects functional integration with cardiomyocyte cultures. *Circ Res* 2008;103:167-176.
19. Jalife J. Inward rectifier potassium channels control rotor frequency in ventricular fibrillation. *Heart Rhythm* 2009;6:S44-S48.

20. Jalife J. Deja vu in the theories of atrial fibrillation dynamics. *Cardiovasc Res* 2011;89:766-775.
21. Pandit SV, Berenfeld O, Anumonwo JM, Zaritski RM, Kneller J, Nattel S, Jalife J. Ionic determinants of functional reentry in a 2-D model of human atrial cells during simulated chronic atrial fibrillation. *Biophys J* 2005;88:3806-3821.
22. Weiss JN, Garfinkel A, Karagueuzian HS, Chen PS, Qu Z. Early afterdepolarizations and cardiac arrhythmias. *Heart Rhythm* 2010;7:1891-1899.
23. Schneider T, Martens PR, Paschen H, Kuisma M, Wolcke B, Gliner BE, Russell JK, Weaver WD, Bossaert L, Chamberlain D. Multicenter, randomized, controlled trial of 150-J biphasic shocks compared with 200- to 360-J monophasic shocks in the resuscitation of out-of-hospital cardiac arrest victims. Optimized Response to Cardiac Arrest (ORCA) Investigators. *Circulation*. 2000;102:1780-1787.
24. Janardhan AH, Gutbrod SR, Li W, Lang D, Schuessler RB, Efimov IR. Multistage electrotherapy delivered through chronically-implanted leads terminates atrial fibrillation with lower energy than a single biphasic shock. *J Am Coll Cardiol*. 2014;63:40-48
25. Chen PS, Feld GK, Kriett JM, Mower MM, Tarazi RY, Fleck RP, Swerdlow CD, Gang ES, Kass RM. Relation between upper limit of vulnerability and defibrillation threshold in humans. *Circulation* 1993;88:186-192.
26. Efimov IR, Cheng YN, Biermann M, Van Wagoner DR, Mazgalev TN, Tchou PJ. Transmembrane voltage changes produced by real and virtual electrodes during monophasic defibrillation shock delivered by an implantable electrode. *J Cardiovasc Electrophysiol* 1997;8:1031-1045.
27. Frazier DW, Wolf PD, Wharton JM, Tang AS, Smith WM, Ideker RE. Stimulus-induced critical point. Mechanism for electrical initiation of reentry in normal canine myocardium. *J Clin Invest* 1989;83:1039-1052.
28. Entcheva E. Cardiac optogenetics. *Am J Physiol Heart Circ Physiol* 2013;304:H1179-H1191.
29. Ikeda T, Uchida T, Hough D, Lee JJ, Fishbein MC, Mandel WJ, Chen PS, Karagueuzian HS. Mechanism of spontaneous termination of functional reentry in isolated canine right atrium. Evidence for the presence of an excitable but nonexcited core. *Circulation* 1996;94:1962-1973.
30. Yamazaki M, Honjo H, Ashihara T, Harada M, Sakuma I, Nakazawa K, Trayanova N, Horie M, Kalifa J, Jalife J, Kamiya K, Kodama I. Regional cooling facilitates termination of spiral-wave reentry through unpinning of rotors in rabbit hearts. *Heart Rhythm* 2012;9:107-114.
31. Zsebo KM, Yaroshinsky A, Rudy JJ, Wagner K, Greenberg B, Jessup M, Hajjar RJ. Long Term Effects of AAV1/SERCA2a Gene Transfer in Patients with Severe Heart Failure: Analysis of Recurrent Cardiovascular Events and Mortality. *Circ Res* 2014;114:101-108.
32. Ahmari SE, Spellman T, Douglass NL, Kheirbek MA, Simpson HB, Deisseroth K, Gordon JA, Hen R. Repeated cortico-striatal stimulation generates persistent OCD-like behavior. *Science* 2013;340:1234-1239.
33. Tye KM, Prakash R, Kim SY, Fenno LE, Grosenick L, Zarabi H, Thompson KR, Gradinaru V, Ramakrishnan C, Deisseroth K. Amygdala circuitry mediating reversible and bidirectional control of anxiety. *Nature* 2011;471:358-362.

Supporting information

Methods

Optical mapping of intracellular [Ca^{2+}]

The effects of Catch activation on intracellular Ca^{2+} concentrations and dynamics were assessed by optical mapping using Rhod-2-AM (Life Technologies, Bleiswijk, the Netherlands) as calcium-sensitive dye. To this purpose, neonatal rat atrial cardiomyocyte (aCMC) cultures were incubated with 2.5 μM Rhod-2-AM in Dulbecco's modified Eagle's medium/HAM's F12 (DMEM/F12; 1:1, v/v; Life Technologies at 37°C for 30 minutes, after which cells were rinsed with DMEM/F12 to remove excess dye. Subsequently, cells were kept in the incubator for another 30 minutes to allow de-esterification of internalized AM esters after which optical signals were captured using the MiCAM ULTIMA-L imaging system (SciMedia, Costa Mesa, CA). During optical mapping of [Ca^{2+}], cells were stimulated electrically with an epoxy-coated bipolar platinum electrode by delivery of 3 square suprathreshold electrical stimuli at 1000-ms intervals (1 Hz) prior to exposure to a 500-ms blue light pulse. Electrical pacing at 1 Hz was re-initiated 10, 20, 50, 100, 200, 500 and 1000 ms after the blue light had been switched off. The amplitude of the calcium transient, the basal Ca^{2+} signal and the occurrence of propagated calcium waves were analyzed using BrainVision Analyzer 1101 software (Brainvision, Tokyo, Japan).

Results

Optical mapping setup and light-emitting diode (LED)-induced shift in optical signal baseline

Using the setup depicted in Supplementary material online, *Figure S1A*, exposure of untransduced and unstimulated neonatal rat atrial cell cultures to blue light LED caused an immediate vertical drop in baseline optical signal (Supplementary material online, *Figure S1B*). The amplitude of the decrease in baseline optical signal depended on the light intensity. The temporal precision of the LED control by the pacing module was checked by calculating the exposure times detected by the charge-coupled device (CCD) camera. Upon a 500-ms blue light pulse, 94% of pixels showed an exposure time of 504 ms while for the remainder of the pixels the exposure time was 510 ms, exemplifying the tight control of the LED by the pacing module (Supplementary material online, *Figure S1C*). During reentry, optical signal baseline showed a similar downward shift as seen in the absence of activation. Importantly,

during the downward shift (LED-on period) the action potential (AP) morphology remained unchanged (Supplementary material online, *Figure S1D*). Offline adjustment of the baseline during the LED-on period did not principally alter optical signal distribution through the culture (Supplementary material online, *Figure S1E*). Thus, the optical mapping setup allowed direct correlation of events during the LED-on period with changes in electrophysiological parameters.

Electrophysiological effects of 500-ms light pulses on LV.CatCh~eYFP↑-transduced aCMC cultures

Because CatCh is permeable to Ca^{2+}, prolonged light exposure could lead to perturbations in intracellular Ca^{2+} in LV.CatCh~eYFP↑-transduced cultures, while the Na^{+} permeability of CatCh could lead to a decrease in excitability. As both effects, if persisting after turning off the LED, could be proarrhythmic, we tested the electrophysiological effects of the 500-ms blue light pulse used for termination of spiral wave reentry. To this purpose, aCMC cultures were paced electrically at 1 Hz prior to exposure to a 500-ms blue light pulse, during optical mapping using Rhod-2AM as Ca^{2+}-binding dye (n=10) or di-4-ANEPPS (n=10) as a voltage-sensitive dye. Electrical pacing at 1 Hz was resumed 10, 20, 50, 100, 200, 500 and 1000 ms after turning off the blue LED. Comparison of the calcium transients prior to and after exposure to blue light did not reveal significant differences irrespective of the length of the LED off-to-electrical pacing interval (*Figure S4A,B*). Calcium transient amplitude after exposure to blue light was not significantly different from that before CatCh activation (100% vs 100.2±4.6% after light exposure)(*Figure S4C*). In addition, no propagated Ca^{2+} waves were found after the LED-on period. In 1 culture, reentry was induced by electrical pacing starting at 10 ms after the LED was turned off. In this particular case, pacing most likely occurred in the vulnerable window after repolarization from the LED-induced depolarizing current instead of being caused by perturbations in intracellular Ca^{2+} as no (propagated) calcium waves or reexcitations were found after exposure to a 500-ms blue light pulse (*Figure S4A,B,D*). In addition, conduction velocity, AP duration at 80% repolarization (APD_{80}) and AP amplitude in LV.CatCh~eYFP↑-transduced aCMC cultures prior to light exposure did not significantly differ from those after exposure to blue light (conduction velocity: 100 vs 101.7±19.5% post LED-on, APD_{80}: 100 vs 103.4±10.5% after light exposure and AP amplitude: 100 vs 102.0±11.1% post LED-on) (*Figure S4E,F,G*). Together, these results indicate that prolonged (*i.e.* 500 ms) light exposure of LV.CatCh~eYFP transduced↑-cultures, at the given conditions, does not cause pro-arrhythmicity due to persistent electrophysiological disturbances.

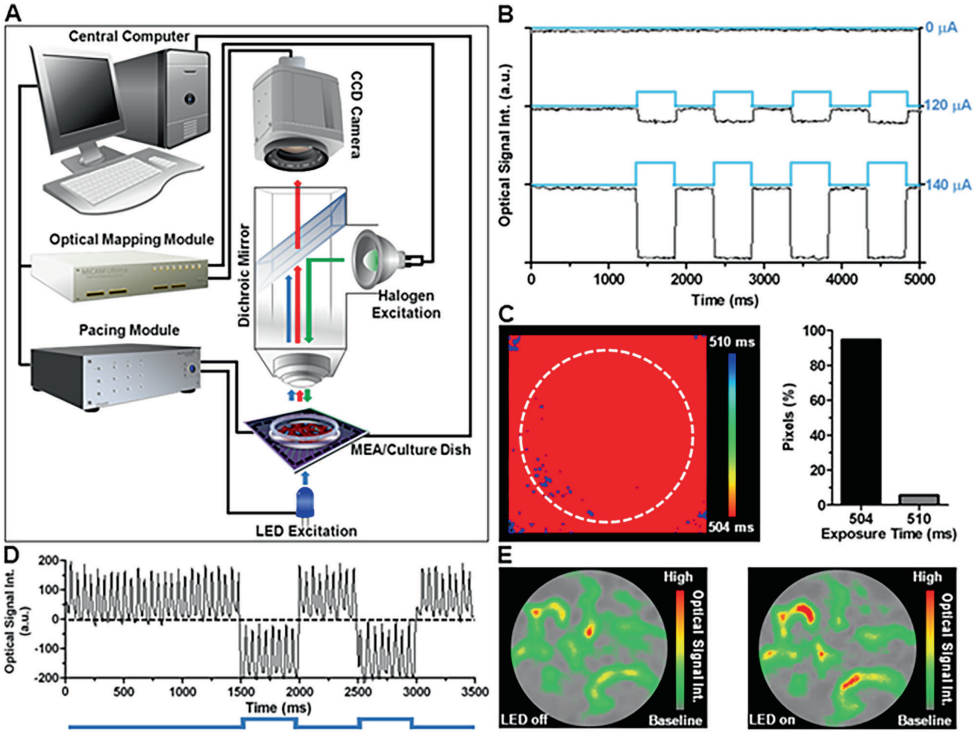

Supplementary Figure S1. *Mapping setup and LED-induced shift in optical signal baseline*. (*A*) Schematic representation of the mapping setup. (*B*) Examples of optical signal traces during exposure of an atrial culture to 500-ms blue LED light pulses of different intensities by changing the current input generated by the pacing module from 0 (upper lines) to 120 (middle lines) and 140 (lower lines) µA, showing that the magnitude of the decrease in baseline optical signal depends on the intensity of the blue light. (*C*) Exposure map and quantification of the exposure time per pixel of the charge-coupled device (CCD) camera measured at 6-ms intervals, showing exposure times of 504 and 510 ms for 94 and 4% of the pixels, respectively. (*D*) Typical example of an optical signal trace of an atrial culture during reentry induced by electrical burst pacing followed by exposure to two subsequent 500-ms blue LED light pulses, demonstrating that the drop in the baseline of the optical signal coincides with the exposure to blue light. The signal morphology remains unchanged, enabling direct read-out of the LED-on period in the optical mapping trace. (*E*) Snap shots of the optical signal in an atrial culture during reentry without exposure to blue light (left panel), and during exposure to blue light after correction of the baseline-drop artifact (right panel), showing similar optical signal distributions immediately before and 250 ms after the LED was turned on. MEA, multi-electrode array; a.u., arbitrary units.

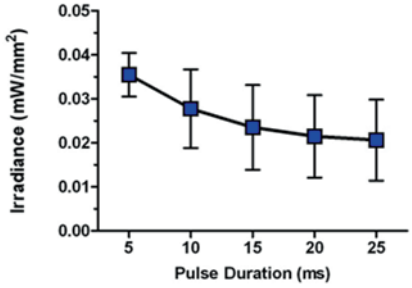

Supplementary Figure S2. *Strength-duration analysis of optical pacing threshold.* Quantification of the average minimal irradiance necessary to elicit an AP at pulse durations of 5, 10, 15, 20 and 25 ms in LV.CatCh~eYFP↑-transduced aCMC cultures (n=8).

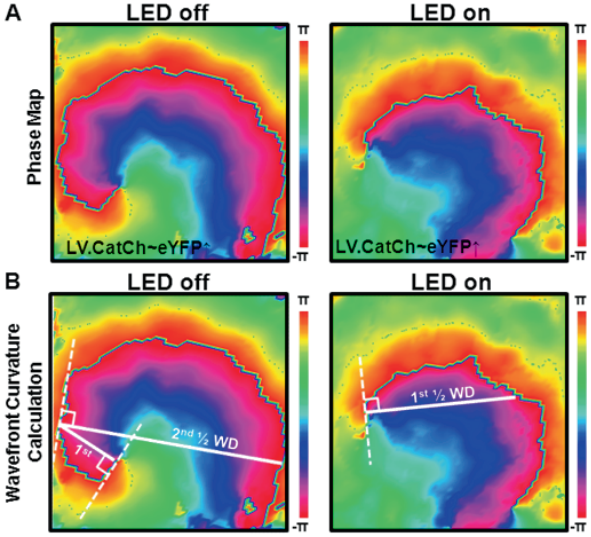

Supplementary Figure S3. *Wavefront curvature analysis. (A)* Typical examples of phase maps of an LV.CatCh~eYFP↑-transduced aCMC culture before (left panel) and during (right panel) exposure to blue light. *(B)* The same phase maps as depicted in subfigure A including the lines used to measure the wavefront curvature. Dashed white lines represent tangent lines along the wavefront near the phase singularity. Uninterrupted white lines, perpendicular to the tangent line, represent the distance between the spiral wave tip and the wavefront at half winding (1st ½ WD). This shows that the 1st ½ WD is typically less than half of the second half winding distance, indicating an increase in wavefront curvature towards the phase singularity (left panel). The 1st ½ WD is increased during light exposure (right panel) indicating a decrease in wavefront curvature near the core.

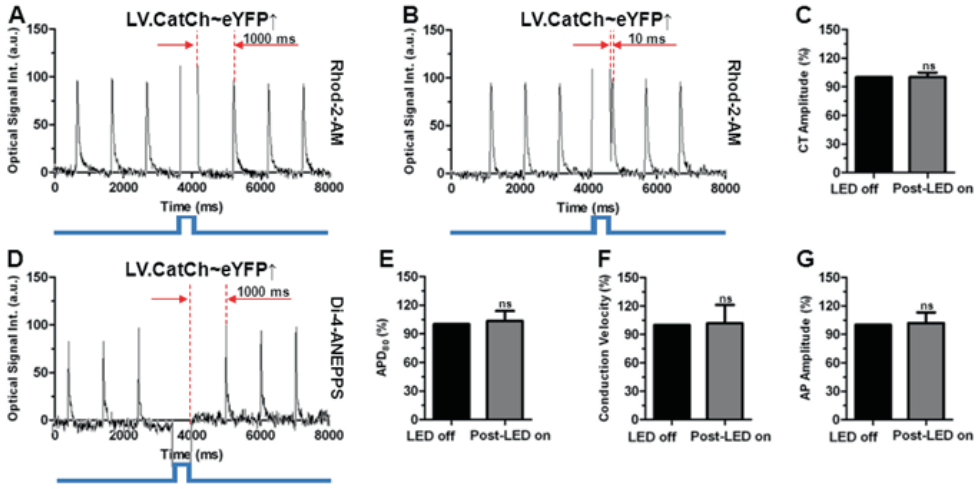

Supplementary Figure S4. *Electrophysiological effects of 500-ms light pulses on LV.CatCh~eYFP↑-transduced aCMC cultures*. (*A*,*B*) Typical examples of the Rhod-2-AM optical signals in 1-Hz electrically paced LV-CatCh~eYFP↑-transduced aCMC cultures before and after exposure to a 500-ms blue light pulse. Electrical stimulation was resumed 1000 ms (*A*) or 10 ms (*B*) after turning off the LED. (*C*) Quantification of calcium transient (CT) amplitude based on Rhod-2AM mapping. (*D*) Example of the di-4-ANEPPS optical signal in an LV.CatCh~eYFP↑-transduced aCMC culture before and after exposure to a 500-ms blue light pulse. Electrical stimulation was resumed 1000 ms after turning off the LED. Quantification of (*E*) AP duration at 80% repolarization (APD_{80}), (*F*) conduction velocity and (*G*) action potential (AP) amplitude, based on voltage-sensitive dye mapping, after exposure to blue light as a percentage of these characteristics prior to exposure to light. ns: non-significant vs LED off using a Wilcoxon signed rank test.

Supplementary Movie 1 Typical example from an optical mapping experiment in a neonatal rat aCMC culture transduced with LV.CatCh~eYFP↑ during light-induced termination of spiral wave reentry. The upper part shows the high-pass-filtered optical signal in a 5-mm^2 square in the culture during spiral wave reentry induced by burst pacing, followed by a 500-ms blue light pulse causing spiral wave termination by a phase singularity-boundary collision. Note: High-pass-filtering caused the blue light-dependent downward shift in optical signal baseline to change into two short (±18 ms duration) artifacts occurring when the LED is turned on and when the LED is turned off only. The lower part displays the corresponding spatially filtered optical AP progression prior to, during and after light-induced spiral wave termination.

Supplementary Movie 2 Typical example from an optical mapping experiment in a neonatal rat aCMC culture transduced with LV. CatCh~eYFP↑ during light-induced termination of spiral wave reentry. The upper part shows the high-pass-filtered optical signal in a 5-mm^2 square in the culture during spiral wave reentry induced by burst pacing, followed by a 500-ms blue light pulse causing spiral wave termination by a phase singularity-phase singularity collision. Note: High-pass-filtering caused the blue light-dependent downward shift in optical signal baseline to change into two short (±18 ms duration) artifacts occurring when the LED is turned on and when the LED is turned off only. The lower part displays the corresponding spatially filtered optical AP progression prior to, during and after light-induced spiral wave termination.